Simple method for generating adjustable trains of picosecond electron bunches

P. Muggli* and B. Allen
University of Southern California, Los Angeles, California 90089, USA

V. E. Yakimenko, J. Park, M. Babzien, and K. P. Kusche
Brookhaven National Laboratory, Upton, Long Island, New York 11973, USA

W. D. Kimura
STI Optronics, Inc., Bellevue, Washington 98004, USA
(Received 12 February 2010; published 20 May 2010)

A simple, passive method for producing an adjustable train of picosecond electron bunches is demonstrated. The key component of this method is an electron beam mask consisting of an array of parallel wires that selectively spoils the beam emittance. This mask is positioned in a high magnetic dispersion, low beta-function region of the beam line. The incoming electron beam striking the mask has a time/energy correlation that corresponds to a time/position correlation at the mask location. The mask pattern is transformed into a time pattern or train of bunches when the dispersion is brought back to zero downstream of the mask. Results are presented of a proof-of-principle experiment demonstrating this novel technique that was performed at the Brookhaven National Laboratory Accelerator Test Facility. This technique allows for easy tailoring of the bunch train for a particular application, including varying the bunch width and spacing, and enabling the generation of a trailing witness bunch.

DOI: 10.1103/PhysRevSTAB.13.052803 PACS numbers: 29.27.Eg, 41.75.Ht, 41.85.Ct

I. INTRODUCTION

In recent years there has been an increasing interest and demand for single as well as trains of ultrashort (picosecond and femtosecond) electron bunches for application to free electron lasers (FELs) [1], x-ray generation [2], plasma wakefield accelerators (PWFA) [3–5], and other advanced schemes such as the particle acceleration by stimulated emission of radiation [6]. The method most widely used to generate short electron bunches is compression of an energy-chirped bunch in a magnetic chicane [7]. Velocity bunching [8,9] is also an effective way of producing short, high brightness beams. It was shown that the inverse free electron laser (IFEL) effect can produce a train of ≈ 150, ≈ 3 fs long bunches separated by ≈ 30 fs, the period of the CO_2 laser pulse that drives the IFEL [10]. IFEL interaction at the 7th harmonic of the undulator resonant wavelength has also produced trains of bunches with ≈ 30 fs spacing [11].

Illuminating the rf-gun photocathode with multiple laser pulses [12] (within the same rf period) or a laser pulse with a beat frequency [13] are other methods that have been proposed to create a train of (sub)picosecond electron bunches. These methods have been explored for THz radiation generation [14]. Space charge effects at the photocathode seem to impede the bunch train formation. However, the bunch train structure can be recovered at higher beam current after a longitudinal plasma oscillation driven by a radio frequency or a magnetic compressor [15,16].

For some applications it is desirable to be able to tailor the spacing between bunches, as well as their individual length and charge. For example, one way to increase the accelerating field driven by an electron bunch in a PWFA (or in any collinear accelerator) is to modulate the current of the drive bunch and to resonantly drive the wakefield in a high-density plasma. In this case, the plasma wavelength λ_{pe} must be equal to the bunch spacing Δz, i.e., $\Delta z = \lambda_{pe} = 2\pi c/(n_e e^2/\epsilon_0 m_e)^{1/2}$ [17], where n_e is the plasma density, e and m_e the charge and mass of the electron, respectively, and ϵ_0 the permittivity of vacuum. While this resonant excitation maximizes the accelerating wakefield amplitude, the transformer ratio, and therefore the energy transfer efficiency (from the drive train to the wakefield or to a trailing witness bunch), can be optimized by using a ramped bunch train method [18]. In that method, the charge is increased along the bunch train to keep the decelerating field the same for all drive bunches. This method has been recently demonstrated in a dielectric loaded accelerator [19]. Moreover, in order to sample the accelerating field it is also desirable to produce a witness bunch that follows the last drive bunch at a distance $\Delta z'$ optimum for acceleration, i.e., $\Delta z' \cong (n + 1/2)\lambda_{pe}$, $n = 1, 2, \ldots$. The method used here to produce a train of short electron bunches, and first demonstrated by Muggli *et al.* in [20], is similar to that described in Ref. [21] to generate subfemtosecond x-ray pulses in a free electron laser (FEL). A mask is placed in a region of the beam line where the

*muggli@usc.edu

beam is dispersed in energy and its transverse size is dominated by its correlated energy spread. The parts of the beam that hit the solid part of the mask experience large emittance growth, and in the FEL case only the short unspoiled time slice lases in the undulator, after the dispersion is brought back to zero. In the method presented here, the time slices with their emittance spoiled are lost along the beam line, while those with their emittance preserved form the individual bunches in the train. Note that this method relies on emittance spoiling rather than partial or total energy loss by the particles in the mask. That method was proposed in Ref. [22] to modulate the current of an electron bunch in order to significantly reduce the gain length of a FEL lasing in the infrared range. Recently another masking method using a mask and time phase space rotation was suggested to generate tailored trains of bunches [23].

The method used here is very attractive because of its simplicity and because it offers the possibility of tailoring the bunch train for specific applications. The width and the spacing between bunches are controlled by the mask pattern and beam parameters at the mask location, and need not be recurrent. Its implementation is also relatively straightforward since most of today's electron beam lines have either a magnetic chicane or a dogleg. The bunch train structure is very stable in time and energy because the mask is a fixed object in a dispersive section of the beam line. The mask method can be applied at the GeV energy level of a multi-GeV linac, where thanks to adiabatic damping of the emittance, beams can be focused to tighter transverse sizes than in this work ($E_0 = 58$ MeV). Even though the method leads to a significant bunch charge loss ($> 50\%$ for PWFA applications), this loss occurs at low energy when compared to the final energy, and therefore does not significantly affect the efficiency of a high-energy linac. Another benefit of this method is that it can also be used with positron bunches, for example, in the context of a plasma-based e^-/e^+ linear collider.

In this paper, we present detailed experimental results obtained at the Brookhaven National Laboratory (BNL) Accelerator Test Facility (ATF) that demonstrate the validity of the proposed masking method to produce trains of subpicosecond electron bunches that can be tailored for various applications. These results complement those presented in the recent demonstration publication [20]. First, we briefly describe the ATF beam line in Sec. II, and present the method to produce a train of short electron bunches with variable bunch spacing, length, and number [20] in Sec. III. We describe its implementation at the ATF and the bunch structure in space or energy in Sec. IV. In Sec. V we introduce the coherent transition radiation (CTR) diagnostic and analyze the bunch structure in time. In Sec. VI we discuss the application of the masking technique to PWFA experiments. Finally, in Sec. VII we present ways to enhance the method utility as well as other possible applications.

II. ATF BEAM LINE

At the ATF, the electron beam is produced in a 1.6 cell, S-band rf photoinjector [24] and is followed by a 70 MeV, S-band linac. The electron bunch with a typical normalized emittance $\epsilon_{Nx,y}$ of ≤ 2 mm mrad and charge $Q_0 \approx 500$ pC can be sent to three different beam lines. For the present experiment, the beam is directed to ATF beam line 2 using two dipoles and five quadrupoles arranged in a dogleg configuration, as seen in Fig. 1. The simulated beam beta functions $\beta_x = \gamma_0 \sigma_x^2/\epsilon_{Nx}$ and $\beta_y = \gamma_0 \sigma_y^2/\epsilon_{Ny}$ as well as the magnetic dispersion η_x ($\eta_y = 0$) are also shown in Fig. 1. These parameters have been measured at various locations of interest for these experiments, and were found to be within 10% of the calculated values. In the linac, the beam is also accelerated off the crest of the rf wave in order to impart a correlated energy spread on the bunch (typically $\Delta E/E_0 \approx \pm 0.5\%$–$3.5\%$).

In the present experiments the beam energy is $E_0 = 58$ MeV ($\gamma_0 = E_0/mc^2 + 1 \cong 115$). The dogleg quadrupoles are adjusted to obtain two regions of large dispersion and low beta function (in the plane of dispersion) where the transverse beam size σ_x along the horizontal x axis is therefore dominated by the energy spread. The beam line includes a limiting slit aperture installed at the first region along the dogleg (left-hand side dashed line in Fig. 1, $s = 10.8$ m, s the distance along the beam line). This slit with a variable center and width can be used to limit the energy spectrum of the bunch downstream along the beam line. The mask is placed in the second region, at approximately

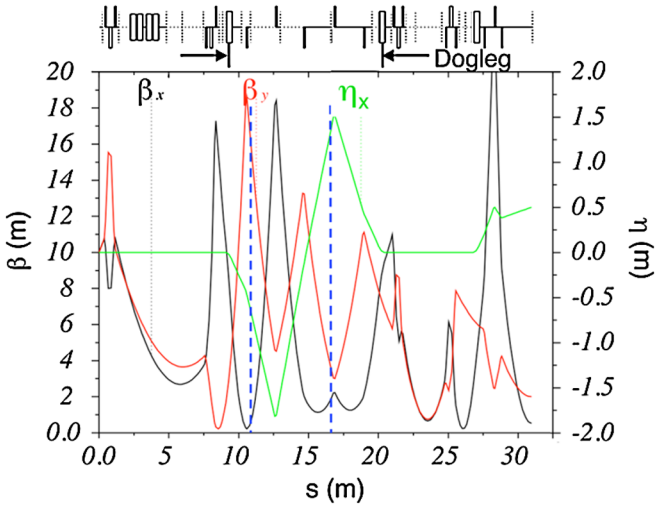

FIG. 1. (Color) Beam beta functions (β_x black line, β_y red line), and dispersion in the x plane η_x (green line) obtained using the MAD program. The beam line elements are shown in the figure above the graph. Quadrupoles focusing in the x (y), horizontal (vertical) direction are indicated by thin rectangles above (below) the middle line, dipoles by full rectangles across the middle line, and beam profile monitors by the dotted lines. The blue dashed lines represent the location of the energy slit (left-hand side line) and of the mask (right-hand side line).

$s = 16.6$ m in Fig. 1. After exiting the dogleg, the beam propagates over a dispersion-free distance of ≈ 6.5 m, where experiments can be performed, before entering a magnetic spectrometer. Before the dogleg, the bunch L_z is about 1650 μm long (or ≈ 5.5 ps, full width of the core). The dogleg longitudinal dispersion function R_{56} is ≈ -4 cm, which means that the effect of the dogleg is to either compress or stretch the bunch by ± 400 μm (or ± 1.3 ps) per percent of correlated energy spread, depending on the sign of the spread (or slew). A bunch with higher (lower) energy particles in the front (back) is compressed (stretched) by the dogleg, and therefore has a positive (negative) correlated energy spread: $\Delta E/E_0 > (<) 0$. The dogleg R_{56} is defined as: $R_{56} = \int ds' \frac{\eta(s')}{\rho(s')}$, where $\rho(s')$ is the local radius of curvature of the beam trajectory.

III. METHOD FOR BUNCH TRAIN GENERATION

For the purpose of creating the bunch train, the incoming bunch is given an energy/time (E, t) correlation $\Delta E/E_0$, where the energy chirp can in principle be chosen positive or negative. For the current set of experiments it is negative and the bunch is stretched by the dogleg. After exiting the linac, the bunch enters the dogleg section of the beam line where the magnetic dispersion is not zero. Therefore in the dogleg, the (E, t) correlation acquired by the bunch in the linac also corresponds to an energy/transverse space (E, x) correlation. To produce a train of short bunches, a mask is inserted in the beam path (see Fig. 2) at the second dogleg location where the beam transverse size in the x plane is dominated by the correlated energy spread. The beam electrons that hit the solid part of the mask suffer multiple scattering, and as a result, energy (and therefore also time) slices of the bunch see their emittance greatly spoiled. Afterwards these slices are lost along the beam line. However, beam slices that pass in the mask gaps preserve their emittance, and travel to the end of the beam line.

At the end of the dogleg, the magnetic dispersion is brought back to zero, and the (E, x) correlation is removed and only the (E, t) correlation remains. The mask spatial pattern imprinted on the bunch therefore determines the bunch train time pattern. The mask pattern can thus be designed to produce, for example, a train of equidistant drive bunches followed by a witness bunch for PWFA experiments. The width and spacing of the bunches are determined by the beam and mask characteristics as explained below. The number of bunches can be selected through the high-energy slit aperture. One obvious consequence of this mask technique is the loss of the charge that hits the mask material. For PWFA applications (see Sec. VII) this loss is $\approx 50\%$ and is similar to that in the case of bunching by an IFEL, where the maximum bunching efficiency is only 50% and the rest of the charge remains in a continuous background [11,25].

The linac rf wave amplitude curvature can cause the bunch head-to-tail energy correlation not to be strictly linear. However, this nonlinearity has little effect on the results when the correlated energy spread is chosen such that the bunch is stretched by the dogleg R_{56} ($\Delta E/E_0 < 0$), as confirmed by the results presented here. Moreover, once known, this curvature can in principle (if not too strong) be compensated for by the mask pattern.

For these experiments the mask is a mesh made of steel wires with diameter d spaced by a distance D (center to center) and stretched on a frame as shown in Fig. 3. The mask is inserted at $s = 16.6$ m in Fig. 1. The total transverse root-mean-square (rms) beam size σ_x in the plane of dispersion at the mask location is given by the beam betatron size $[(\beta_x \epsilon_{Nx}/\gamma_0)^{1/2}]$ and the dispersed size

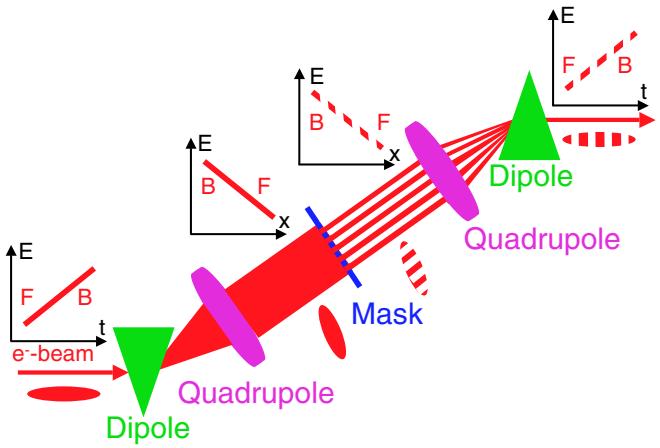

FIG. 2. (Color) Simplified schematic of the mask principle. Only the dogleg section of the beam line and two quadrupoles are pictured (not to scale). The side graphs represent the beam energy correlation with the beam front labeled by F and the back by B.

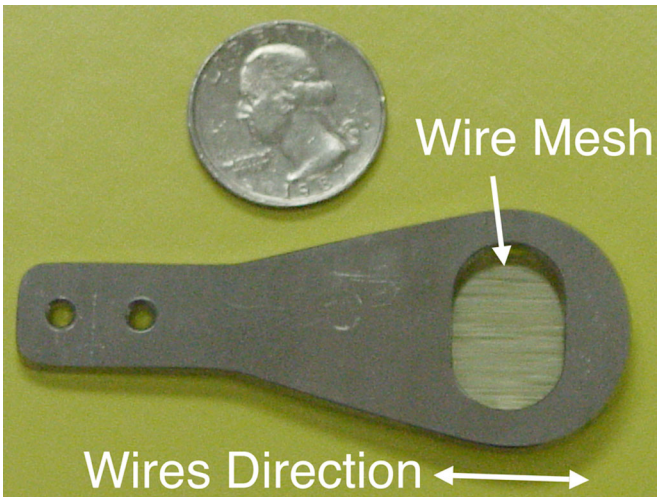

FIG. 3. (Color) Picture of the mask showing the frame supporting the wires with diameter $d = 500$ μm and period $D = 1.27$ mm. The steel wires are approximately horizontal in the picture and vertical in the experiment.

($\eta_{\mathrm{mask}}\frac{\Delta E}{E_0}$) added in quadrature:

$$\sigma_x = \sqrt{\frac{\beta_x \epsilon_{Nx}}{\gamma_0} + \left(\eta_{\mathrm{mask}}\frac{\Delta E}{E_0}\right)^2}. \quad (1)$$

Figure 1 shows that at the mask location $\beta_x \cong 1.90$ m, and the emittance contribution [first term in Eq. (1)] is $\sigma_{x\beta} = (\beta_x \epsilon_{Nx}/\gamma_0)^{1/2} \cong 182\ \mu$m ($\epsilon_{Nx} = 2$ mm mrad, $\gamma_0 = 115$). At the same location the dispersion is $\eta_{\mathrm{mask}} = 1.37$ m and the dispersion contribution to the rms beam size [second term in Eq. (1)] is $\sigma_{x\eta} = \eta_{\mathrm{mask}}\Delta E/E_0 \cong 13.7$ mm for $\Delta E/E_0 = 1\%$. The beam size at the mask is therefore dominated by the dispersion term, as desired. Note that this condition is also satisfied at the energy slit location where $\eta_{\mathrm{slit}} \cong 0.6$ m and $\beta_x = 0.41$ m. Additionally, in order for the wires to cast a crisp shadow far downstream from the mask, $\sigma_{x\beta}$ must be smaller than the wires radius: $\sigma_{x\beta} \ll d/2$ (see Sec. IV). The maximum number of (equidistant) bunches N_b that can be produced is [for $\beta_x \epsilon_{Nx}/\gamma_0 \ll (\eta_{\mathrm{mask}}\Delta E/E_0)^2$]

$$N_b = \frac{\sigma_x}{D} \cong \frac{\eta_{\mathrm{mask}}}{D}\left|\frac{\Delta E}{E_0}\right|. \quad (2)$$

This expression assumes that $\sigma_x > D$ or $|\Delta E/E_0| > D/\eta_{\mathrm{mask}}$, i.e., the dispersed beam intercepts more than one wire. The absolute value is used to ensure that $N_b > 0$. For a bunch length $L_z' = L_z + R_{56}\Delta E/E_0$ after the dogleg, the wire size and spacing are demagnified by a factor DM:

$$DM = \frac{\sigma_x}{L_z'} \cong \frac{\eta_{\mathrm{mask}}}{L_z'}\left|\frac{\Delta E}{E_0}\right|. \quad (3)$$

Note that the demagnification can also be determined by dividing the wires spacing by the measured distance between bunches Δz: $DM = D/\Delta z$. The number of bunches (and the bunch train length) is controlled by using the energy slit in conjunction with the mask to limit the width of the bunch energy spectrum at the mask.

After the dogleg, the spacing between the bunches Δz (corresponding to a time interval $\Delta t \cong \Delta z/c$) can be written as

$$\Delta z = \frac{L_z'}{N_b}. \quad (4)$$

Therefore

$$\Delta z \cong \frac{D}{\eta_{\mathrm{mask}}}\frac{L_z + R_{56}\Delta E/E_0}{|\Delta E/E_0|}. \quad (5)$$

This expression gives the main dependencies of the spacing between the bunch and the beam and mask parameters. The length of the individual bunches is $T\Delta z = [(D-d)/D]\Delta z$ (when $\sigma_{x\beta} \ll d$), where $T = (D-d)/D$ is the mask transparency (in space or time). It is interesting to note that in this case, whether the bunch is compressed or stretched by the dogleg R_{56}, Δz decreases with increasing $|\Delta E/E_0|$. This is due to the fact that as $|\Delta E/E_0|$ increases, the number of mask wires intercepted by the beam also increases in both cases, and the dogleg compression or stretching is small ($R_{56}|\Delta E/E_0| \ll L_z$).

For an incoming bunch with total charge Q_0, the average charge per bunch Q_b is

$$Q_b = T\frac{Q_0}{N_b} \cong \frac{Q(D-d)}{\eta_{\mathrm{mask}}|\Delta E/E_0|}. \quad (6)$$

The bunches average current I_b (after the dogleg) is

$$I_b = \frac{Q_0 c}{L_z'}, \quad (7)$$

the same as the incoming bunch current I_b after the chicane compression or stretching. Again, the above expressions for Δz and Q_b assume that more than one bunch are produced, i.e., $\eta_{\mathrm{mask}}|\Delta E/E_0| > D$ and do not take into account the incoming bunch charge or current profiles, but assume constant values. Figure 4 shows the expected bunch spacing Δz as well as the average bunches current I_{mb} and charge Q_b as a function of the correlated energy spread, obtained from the above expressions. Picosecond bunches with 10–100 A current can be generated with $\Delta E/E_0$ of the order of $\pm 0.5\%$ and the ATF parameters. Subpicosecond bunches can be obtained with larger energy spreads, as shown below.

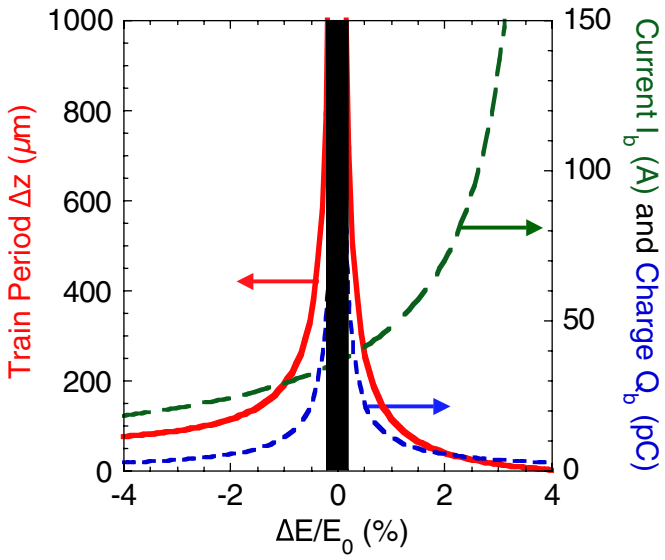

FIG. 4. (Color) Spacing between the electron bunch in the train Δz [Eq. (5), red continuous line], individual bunch current [Eq. (7), green dashed line], and charge [Eq. (6), blue line] as a function of the bunch correlated energy spread $\Delta E/E_0$. Negative values of $\Delta E/E_0$ lead to stretching of the bunch by the chicane with $R_{56} < 0$. The black rectangle covers $|\Delta|E/E_0| < 0.2\%$ for which a train of only one bunch is produced.

IV. BUNCH TRAIN STRUCTURE IN SPACE

Figure 5 shows a downstream-looking view of the beam at the energy slit. The fraction of the beam removed by the slit at low and high energies is visible, while the rest of the beam travels through the slit to the mask. In this case the total correlated energy spread is $\Delta E/E_0 \approx -1\%$, while the slits limits it to $\approx -0.5\%$ centered around $E_0 = 58$ MeV.

Figure 6 shows the corresponding bunch energy spectrum (red curve) recorded in the spectrometer plane at the end of the beam line ($s = 31$ m) for the case of a steel wire mask with $d = 0.5$ mm and $D = 1.27$ mm. Note that the relative amplitude of the individual bunches reflects the incoming bunch charge or current distribution, as can be verified by removing the mask. At this location, the magnetic dispersion is $\eta \cong 0.5$ m (see Fig. 1). Six bunches are clearly visible, confirming that the mask shadow (in energy) is cast all the way along the beam line. This figure also shows a spectrum for the case of an energy slit width of $\approx 0.6\%$ (green curve), showing seven bunches (one added with respect to the previous case), and demonstrating the ability to independently control the number of bunches in the train using the limiting energy slit. Figure 6 shows that ≈ 14.5 m away from the mask, the scattered particles are lost. Electrons hitting the wires are scattered by a rms angle $\theta_{\rm rms}$ [26]:

$$\theta_{\rm rms} = \left(\frac{4\pi}{\alpha}\right)^{1/2} \frac{mc^2}{p_0 c \beta_0} \left(\frac{L}{L_R}\right)^{1/2} \cong \frac{21.2}{E_0\ ({\rm MeV})} \left(\frac{L}{L_R}\right)^{1/2}, \tag{8}$$

where L_R is the radiation length of the material, $\beta_0 = (1 - 1/\gamma_0^2)^{1/2}$ (≈ 1 for $\gamma_0 = 115$), $p_0 = E_0/c$ is the relativistic particles momentum, and $\alpha \cong 1/137$ is the fine structure constant. The radiation length for steel is $L_R = 1.75$ cm and the wires are only $\approx L_R/35$ thick. Hence, no significant energy loss ($\approx 3\%$) is occurring, but large scattering is expected. The maximum scattering angle is $\theta_{\rm rms} \cong 62$ mrad. The beamlets hitting the solid parts of the mask see their emittance grow by a factor of the order of

$$\frac{\epsilon_{N\rm out}}{\epsilon_{N\rm in}} \cong \left(1 + \frac{\beta_x}{\gamma_0 \epsilon_{N\rm in}} \theta_{\rm rms}^2\right)^{1/2}. \tag{9}$$

This factor is obtained by adding the emittance growth $\sigma_{x\beta}\theta_{\rm rms}$ in quadrature to the incoming emittance. The emittance grows by a factor of more than 600. Note that it takes only 10 μm of steel to spoil the emittance by a factor of 100 ($\epsilon_{N\rm in} = 2$ mm mrad), and this thickness is reached within less than 1 μm of the edge of the 500 μm diameter round wire. Therefore, despite their cylindrical shape, the wires can be considered as square scatterers, and the electrons hitting the wires will be quickly lost along the beam line. The average spacing between bunches on Fig. 6 is 48 pixels (or ≈ 100 keV), while the average width of the peaks is 27 pixels. This corresponds to a period to width ratio of about 1.8, which is smaller than the ratio $D/d \approx 2.5$. This blurring of the mask shadow may be due to the fact that the transverse beam size at the wire ($\sigma_{x\beta} \cong 182$ μm) is not significantly smaller than the wires radius ($d/2 = 250$ μm).

The sharpness of the shadow cast by the mask can be estimated for the case of the transmission of a bunch with a

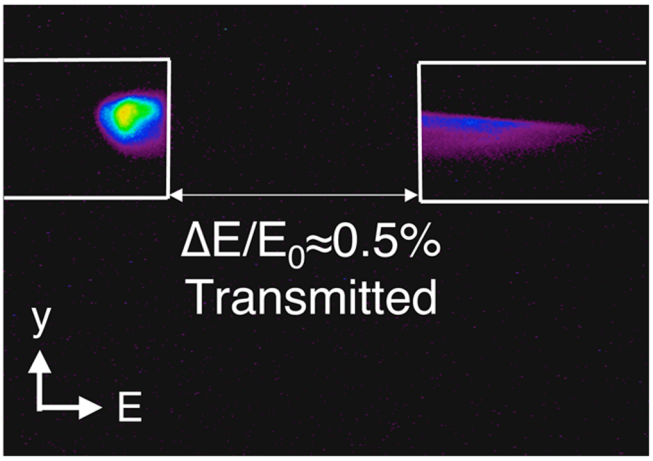

FIG. 5. (Color) Raw video image of the beam at the energy slit ($s = 10.8$ m in Fig. 1) looking downstream from the electron gun. The part of the beam visible on the picture is intercepted by the slit. The slit jaws are indicated by the white rectangles. The transmitted energy range is $|\Delta E/E_0| \approx 0.5\%$ around the $E_0 = 58$ MeV average energy.

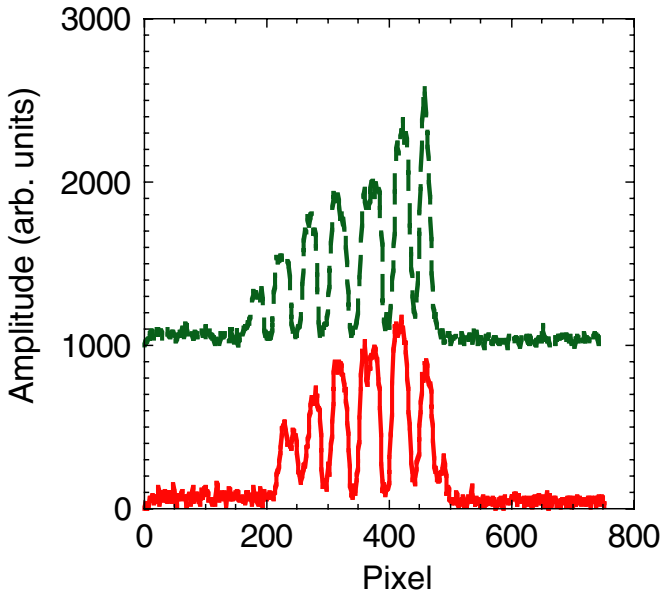

FIG. 6. (Color) Profiles of the beam dispersed in energy at the end of the beam line ($s = 31$ m in Fig. 1) with the energy slit allowing either six microbunches (red line) or seven microbunches (dashed green line, shifted up in amplitude by 1000 a.u.), which demonstrates the ability to choose the number of microbunches in the bunch train. Variations in the microbunches amplitudes are due to slightly different beam tuning.

Gaussian transverse distribution with an rms width $\sigma_{x\beta}$ incident upon a periodic square wire mask. Assuming that particles hitting the mask are lost, the transmitted fraction T of the charge as a function of the beam centroid position x_0 is given by the convolution of the beam betatron size and the mask shape [27]:

$$T(x_0; x_{w,i}, d, \sigma_x) = 1 - \frac{1}{2}\Big[\sum_i erf\Big(\frac{x_{w,i} + d/2 - x_0}{\sqrt{2}\sigma_{x\beta}}\Big) - erf\Big(\frac{x_{w,i} - d/2 - x_0}{\sqrt{2}\sigma_{x\beta}}\Big)\Big], \quad (10)$$

where $x_{w,i}$ is the position of the i^{th} wire for a mask with equidistant wires $x_{w,i} = iD$, $i = \ldots, -1, 0, +1, \ldots$.

The transmission for a mask with $d/D \approx 0.4$, similar to the ratio in the experiment, is plotted in Fig. 7 for various $\sigma_{x\beta}/(d/2)$. Figure 7 shows that for $\sigma_{x\beta}/(d/2) = 0.01$ the shadow closely follows the mask shape and the bunches are well formed. For $\sigma_{x\beta}/(d/2) = 0.1$ the gap between the bunches starts filling up, while for $\sigma_{x\beta}/(d/2) = 0.5$ the bunch train charge distribution become continuous. For these experiments, $\sigma_{x\beta}/(d/2) = 0.73$, and the modulation is about 0.95:0.2, as shown in Fig. 7. Decreasing the beam emittance to 1 mm mrad would bring $\sigma_{x\beta}/(d/2)$ down to 0.5, and improve the contrast to a continuous distribution almost without background charge.

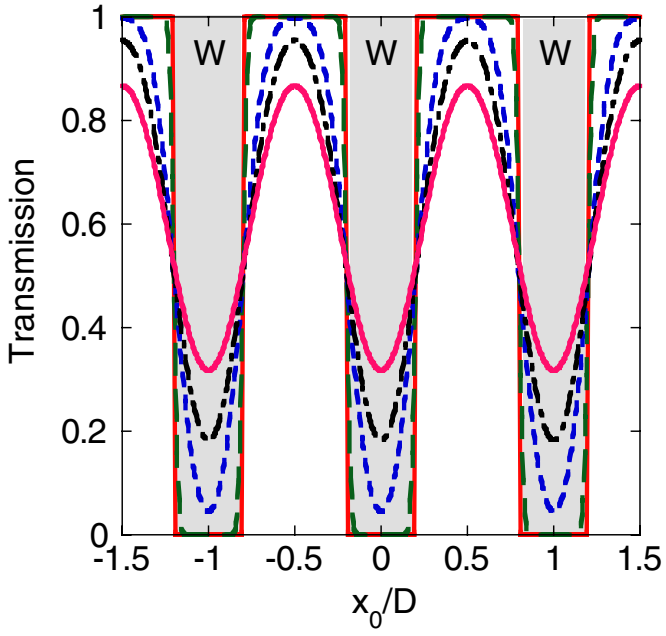

FIG. 7. (Color) Plot of the transmission of a mask [as given by Eq. (10)] with normalized parameters $d/D \approx 0.4$ as a function of the position (corresponding to energy in a dispersive region) of the beam for various ratios of betatron transverse size σ_β to mask wire diameter $\sigma_\beta/(d/2) = 0.01$ (red line). 0.1 (green line), 0.5 (blue line), 0.75 (black line, similar to parameters of Ref. [20]), and 1.0 (pink line). The wires are indicated by shaded regions and the letter W.

One must now prove that between the dogleg and the energy spectrometer, where the magnetic dispersion is zero, the mask pattern measured in the energy plane is indeed transposed into a time pattern.

V. BUNCH TRAIN STRUCTURE IN TIME

The bunch time structure after the dogleg is measured using coherent transition radiation (CTR). It is well known that charged particles emit a broadband spectrum of transition radiation (TR) when traversing the boundary between two media with different dielectric constants [28]. The TR is incoherent for wavelengths much shorter than the typical bunch length ($\lambda_{\text{TR}} \ll \sigma_z$ for a Gaussian bunch with rms width σ_z), while the TR at wavelengths much longer than the typical bunch length ($\lambda_{\text{TR}} \gg \sigma_z$) is coherent. The total TR intensity emitted by a bunch with N_e electrons can be written as

$$I_{\text{tot}}(k) = I_{\text{incoh}} + I_{\text{coh}} = N_e I_e + N_e(N_e - 1) I_e |F(k)|^2, \quad (11)$$

where I_e is the TR intensity emitted by a single electron. The term $|F(k)|^2$ is the norm of the Fourier transform of the longitudinal bunch profile $f(z)$, i.e., $F(k) = (\frac{1}{2\pi})^{1/2} \times \int_{-\infty}^{+\infty} dz f(z) \exp(ikz)$, and is commonly referred to as the longitudinal bunch form factor. It is of the order of unity at long wavelengths ($k \ll 1/\sigma_z$), where the TR signal is dominated by its coherent component. In this regime the CTR signal scales as $N_e(N_e - 1) \approx N_e^2$ for $N_e \gg 1$ (order of 10^9 here).

In principle, information about the bunches length, spacing, and number can therefore be retrieved from the autocorrelation of the bunch train CTR using an interferometer. The interferometer splits the CTR radiation into two components and introduces a path length difference $\Delta\xi$ between the two signals. The two halves of the total CTR electric field $E(t)$ are recombined and the detector measures the time-integrated autocorrelation signal $S(\Delta\xi)$ (square of the sum of the fields):

$$S(\Delta\xi) = \int_{-\infty}^{+\infty} dz \Big(\frac{1}{2}E(z) + \frac{1}{2}E(z - \Delta\xi)\Big)^2. \quad (12)$$

The autocorrelation function $A(\Delta\xi)$ is given by the cross term:

$$A(\Delta\xi) = \frac{1}{2}\int_{-\infty}^{+\infty} dz [E(z)E(z - \Delta\xi)]. \quad (13)$$

For a Gaussian bunch current profile with rms width σ_z, the function A is also Gaussian and has a width equal to $\sqrt{2}\sigma_z$. The autocorrelation function for a train with N_b identical bunches separated by Δz contains $(2N_b - 1)$ peaks separated by Δz with relative amplitudes $1, 2, \ldots, N_b, \ldots, 2, 1$ (i.e., a triangular envelope). In the case of CTR, the electric field is unipolar, and A is therefore a positive function. For a particular bunch train, the

autocorrelator signal can be calculated using Eq. (12). Note that the degree of coherence of the TR is also determined by the transverse bunch form factor [28]. For these experiments the beam at the CTR location is focused to <100 μm, which is smaller than the measured Δz, and this effect can be ignored. The interferometer and detector may introduce some wavelength filtering that can affect the shape of $S(\Delta\xi)$ [Eq. (12)] and $A(\Delta\xi)$ [Eq. (13)].

Figure 8 shows the autocorrelation trace calculated using Eq. (12) and the energy or spatial profile of the six-bunch beam obtained at the end of the beam line (Fig. 6). This represents the autocorrelation trace that would be obtained if the structure observed in the energy plane were transposed into the time domain.

In this experiment, the electron beam emits backward CTR when entering an aluminum mirror placed in the beam path at 45° after the dogleg ($s = 22.6$ m, in Fig. 1). The CTR centered around the beam's specular angle of reflection traverses a ≈ 3 mm thick high-density polyethylene vacuum window (transmission $>60\%$ for $\lambda > 20$ μm), travels through the CTR interferometer, and reflects off a 90° off-axis parabola that focuses the radiation onto a liquid helium-cooled silicon far-infrared bolometer. The signal recorded as a function of the interferometer path length difference is shown in Fig. 9 for the case of a mask with $d = 500$ μm and $D = 1.27$ mm and six bunches (Fig. 6). All the expected 11 peaks are visible in this interferometer scan. They are separated by an average distance of $\Delta z \approx 344 \pm 27$ μm (or $\approx 1.15 \pm 0.09$ ps), as determined from the inset in Fig. 9. Assuming

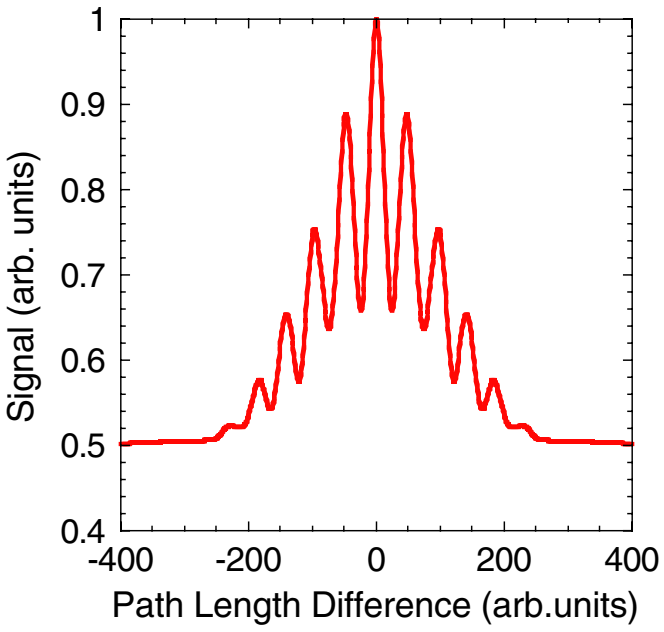

FIG. 8. (Color) Autocorrelation trace calculated from the bunch profile of Fig. 6 with six bunches and using Eq. (12). The horizontal scale is kept arbitrary since it depends on the actual total bunch length after the dogleg.

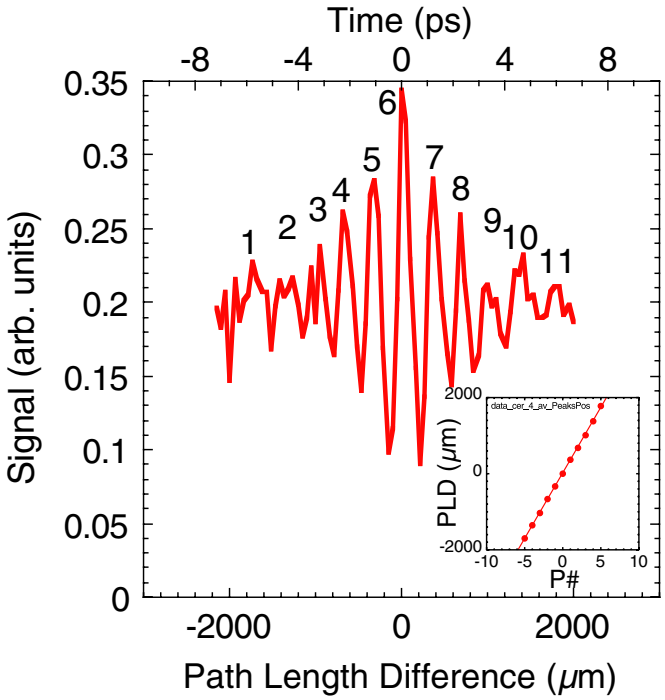

FIG. 9. (Color) CTR interferometer trace for the mask with $d = 500$ μm and $D = 1.27$ mm corresponding to the case of Fig. 6. The distance between the peaks is determined from a linear fit of the measured path length difference (abbreviated PLD) versus peak number (abbreviated *P#*) shown in the inset for the 11 peaks (six bunches). The slope of the curve and therefore the distance between the bunches is about 344 μm.

that the bunches have a square profile, and a width mimicking the mask shape, their length would be $(D - d)/D \approx 0.6$ times narrower than their spacing, corresponding to 208 μm (690 fs). With a total bunch charge of 350 pC before the mask, each bunch contains ≈ 30 pC and hence has a current of ≈ 43 A. The total length of the electron bunch train with six such bunches is therefore of the order of 2270 μm (or ≈ 7.6 ps). For these experiments the bunch was given a correlated energy spread leading to the stretching of its length by the dogleg. The bunch separation is in good agreement with the value of D and the demagnification factor of the system calculated from Eq. (3), i.e., $DM \approx 3.7$ (with $\eta_{\text{mask}} = 1.4$ m and $\Delta E/E_0 \approx -0.5\%$, $L_z = 1650$ μm) and with Eq. (5).

The CTR interferometer trace shown in Fig. 9 has values that dip below the background level (≈ 0.2 in Fig. 9) obtained when the interferometer path length difference is much larger than the length of the bunch train (see Fig. 8). This behavior can be explained by assuming that the overall system does not transport or detect the entire broad CTR spectrum, which in this case extends from wavelengths approximately equal to the bunch width to infinity [see Eq. (11)]. Diffraction and physical apertures restrict the transport of long wavelengths and the cold detector response drops around $\lambda_{\text{cutoff}} = 1000$–$2000$ μm

(long wavelengths cutoff). Calculations of the interferometer signal using Eq. (12) and including a high-pass filter that cuts off wavelengths longer than $\lambda_{\text{cutoff}} = 1000$ μm are shown in Fig. 10 for a train of square bunches. Including the filtering reduces the overall signal and reproduces the dips observed on Fig. 9. Note that this filtering does not affect the determination of the bunch spacing, but essentially prevents the accurate determination of the individual bunch length.

Equation (5) indicates that the bunch spacing can be varied by changing the energy spread imparted to the bunch by the linac. CTR traces were obtained with two different incoming energy spreads: $\Delta E/E_0 = 1.5$ and 3.5% and are shown on Fig. 11. The bunch spacings were determined as in Fig. 9 (see figure inset) and are 434 ± 22 μm and 216 ± 60 μm (or 1.45 ± 0.07 ps and 720 ± 200 fs) for the two respective cases. The case with the shortest Δz has a relatively large error because there are only three bunches in the train. Spacings as small as 150 μm have been achieved. These figures also show once again the ability to choose the number of bunches in the train.

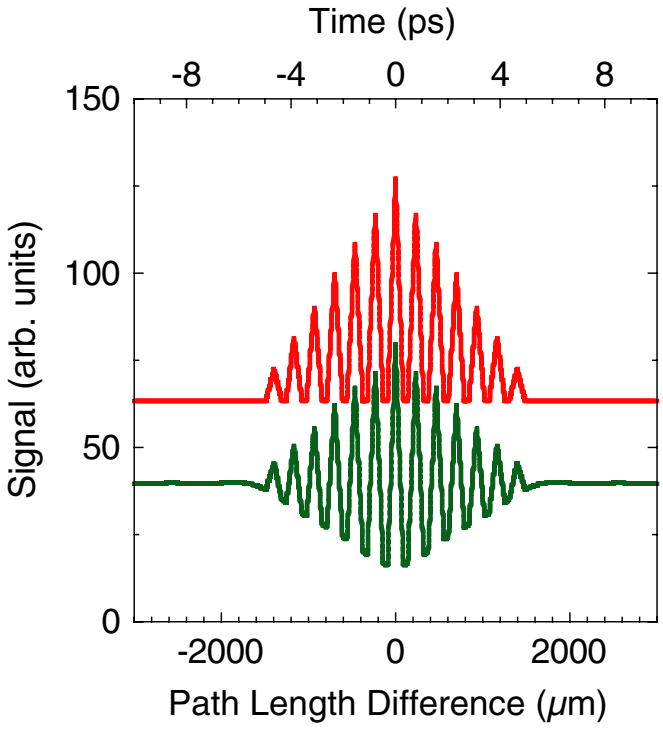

FIG. 10. (Color) CTR interferometer signal calculated using Eq. (12) for the train of six square bunches 208 μm wide and with a 344 μm spacing with the full electric field (red curve) and including a low-pass filter function that cuts off wavelengths shorter than 1000 μm (green curve). The absolute amplitudes are arbitrary, but the relative amplitudes are preserved. The full trace (red curve) has the same features as the expected trace shown in Fig. 8 and the filtered trace (green curve) reproduces the features of the measured signal displayed in Fig. 9.

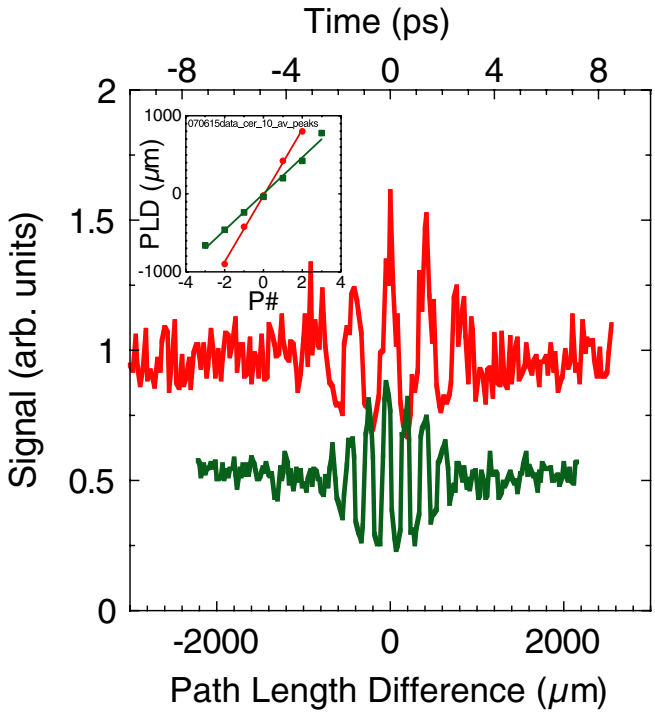

FIG. 11. (Color) Normalized CTR interferometer traces obtained with two different incoming energy spectra: $\Delta E/E_0 = 1.5\%$ (red line, shifted up by 0.5 a.u. after normalization) and 3.4% (green line) and with different energy slit widths leading to three and four bunches, respectively. The dependency of Δz on the incoming energy spread is clearly visible from the two traces. The distance between the peaks is determined from a linear fit of the measured path length difference (abbreviated PLD) versus peak number (abbreviated *P#*) shown in the inset. The slope of the curves is therefore the distance between the bunches.

It is interesting to note that since the CTR interferometer system cuts off the long wavelengths, the unmodulated macrobunch that is not sliced by the mask does not produce any detectable CTR signal since its length is ≈ 2270 μm, which is greater than the detector cutoff wavelength $\lambda_{\text{cutoff}} = 1000$–$2000$ μm. Therefore, inserting a mask that modulates the beam current in time with sufficiently high frequencies allows for the measurement of the long incoming bunch length. This method could be used to deduce the length of long electron bunches emitting CTR in a long wavelength range where detectors are not sensitive.

VI. BUNCH TRAIN FOR PWFA APPLICATIONS

A specific application for a train of bunches is the generation of wakefields for advanced accelerator experiments, for example, in a plasma [3]. In current PWFA experiments, the mask is used in conjunction with the high-energy slit to vary the number of bunches in the train. The drive bunches are equidistant and at resonance separated by one plasma wavelength ($\Delta z = \lambda_{pe}$) [17]. A non-equidistant mask pattern is used to generate a witness

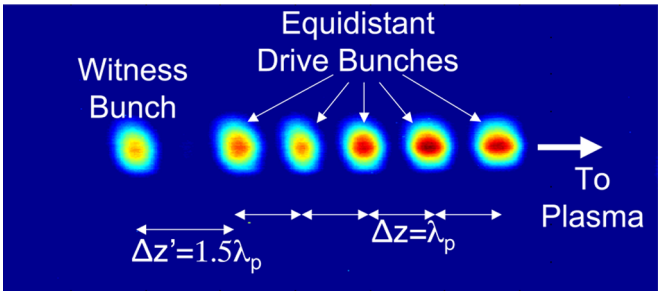

FIG. 12. (Color) Train of bunches for PWFA applications measured in the energy plane: five equidistant drive bunches followed by a witness bunch, with a separation one and a half times that of the drive bunches. CTR measurements show that the same pattern is obtained in time (see Fig. 13).

bunch separated from the last of the equidistant drive bunches by $\Delta z' = 1.5\Delta z$ so that it samples the accelerating wakefield driven by the train containing $N = 1, 2, \ldots, N_{\max}$ bunches. The energy spectrum for the case of five drive bunches and the witness bunch is displayed on Fig. 12. CTR measurements confirm that the same pattern is obtained in time. Figure 13 shows two CTR autocorrelation patterns obtained with two drive bunches, and with the last drive bunch and the witness bunch of Fig. 12, sequentially selected using the energy slit. The inset confirms that the spacing between the last drive bunch and the witness bunch ($\Delta z' \cong 458$ μm in this case) is about 1.5 times the distance between the drive bunches ($\Delta z \cong$ 313 μm), as determined by the mask pattern. Preliminary PWFA results show large energy loss by the drive bunches and possibly energy gain by the witness bunch, both of which are associated with the resonant excitation of the wakefields. These results will be published elsewhere. It is important to study plasma wakes driven by trains of bunches in order to maximize the energy transfer efficiency in a future high-energy plasma-based accelerator by tailoring the bunches charge, as suggested, for example, in Ref. [4].

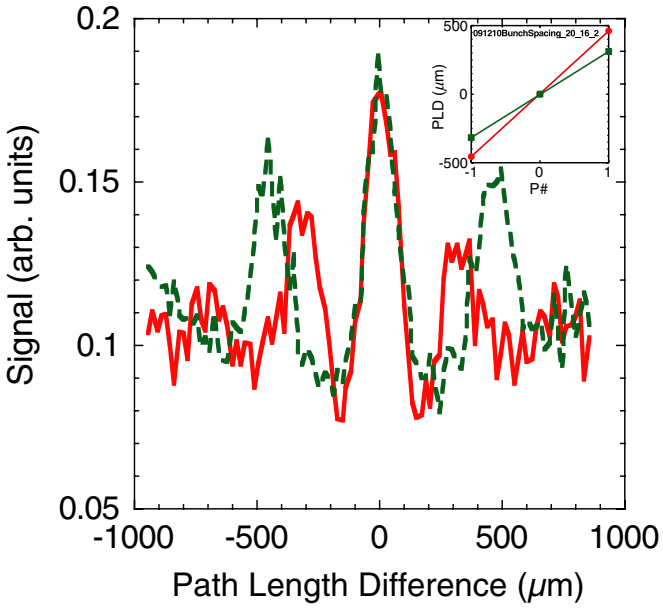

FIG. 13. (Color) Autocorrelation traces obtained with two drive bunches (red continuous line) of Fig. 12, and with the last drive bunch and the witness bunch (green dashed line). The measured interferometer path length difference for each train shows that the spacings are $\Delta z' \cong 458$ μm and $\Delta z \cong 313$ μm, respectively (see inset).

VII. FUTURE WORK

The results presented here demonstrate that placing a mask in a high dispersion, low beta function region of the beam line dogleg produces a temporal bunch train out of a long bunch with a correlated energy spread. The mask and the beam can be tailored for particular applications.

Various modifications can be made to the basic mask design to enhance its capabilities. The bunch spacing Δz can be varied by rotating the mask by an angle θ around the axis of the wires in order to vary the apparent separation distance between the wires, i.e., $D \rightarrow D/\cos\theta$ (d is unchanged, the bunches become shorter). The mask can be designed to compensate for the nonlinear energy chirp the bunch may acquire along the linac. A slit with a wedged width and placed perpendicular to the wires could be used to ramp the charge in the successive bunches in order to maximize the transformer ratio R, defined as the ratio of the peak accelerating field to the peak decelerating field [19]. To improve the contrast ratio between the bunches, another slit placed some distance downstream from the mask could be used to better scrape the particles that saw their emittance spoiled by the mask. The incoming beam emittance can in principle be reduced to 1 mm mrad, and the charge increased to 500 pC, which would generate a sharper, higher current bunch train at the ATF.

Trains of much shorter and higher current bunches could be obtained by using the magnetic chicane available at the ATF in a conjunction with the planned X-band rf cavity [29]. With this compression scheme, the total train length will be a few hundred femtoseconds, limited by the uncorrelated energy spread of the incoming bunch. Note however that since the weakly relativistic electron bunch has a correlated energy chirp, dephasing of the bunches due to energy-dependent time-of-flight differences [$\Delta d \approx (\Delta\gamma/\gamma_0^3)d \ll \Delta z$ for $\Delta\gamma \ll \gamma_0$] will have to be considered and kept smaller than the bunch spacing. These issues will be studied numerically using particle-tracking codes.

This masking method will be used at the Stanford Linear Accelerator Center FACET [30] facility currently under construction, to produce a drive/witness bunch train to demonstrate for the first time the energy doubling of a witness bunch with a narrow (a few percent) energy spread [31].

Finally, besides the PWFA, the bunch trains may find applications for generation of high power THz radiation pulses in dielectric tubes (see for example [32]), for driving large wakefield amplitudes in low group velocity dielectric loaded accelerators [33], for the demonstration of the suppression of the deleterious effect on high brightness beams of coherent synchrotron radiation in dipole magnets [34], as well as for a multiframe femtosecond x-ray camera using inverse Compton scattering of a laser pulse [34]. Plans for experiments to test these applications are underway at the BNL ATF.

ACKNOWLEDGMENTS

This work was supported by the U.S. Department of Energy, Grants No. DE-FG02-04ER41294, No. DE-AC02-98CH10886, No. DE-FG03-92ER40695, and No. DE-FG02-92ER40745. The contribution of the ATF technical staff to this work is greatly appreciated.

[1] A. M. Lindenberg *et al.*, Science **308**, 392 (2005).
[2] M. Cornacchia, in Proceedings of the 18th Particle Accelerator Conference, New York, 1999 (IEEE, New York, 1999), p. 267.
[3] I. Blumenfeld *et al.*, Nature (London) **445**, 741 (2007).
[4] R. Maeda *et al.*, Phys. Rev. ST Accel. Beams **7**, 111301 (2004).
[5] P. Muggli and M. J. Hogan, C.R. Physique **10**, 116 (2009).
[6] S. Banna *et al.*, Phys. Rev. Lett. **97**, 134801 (2006).
[7] M. James *et al.*, IEEE Trans. Nucl. Sci. **30**, 2992 (1983).
[8] L. Serafini and M. Ferrario, in *Physics of, and Science with, the X-Ray Free-Electron Laser*, edited by S. Chattopadhyay, M. Cornacchia, I. Lindau, and C. Pellegrini, AIP Conf. Proc. No. 581 (AIP, New York, 2001), p. 78.
[9] P. Piot *et al.*, Phys. Rev. ST Accel. Beams **6**, 033503 (2003).
[10] Y. Liu, Phys. Rev. Lett. **80**, 4418 (1998).
[11] S. Tochitsky *et al.*, Phys. Rev. ST Accel. Beams **12**, 050703 (2009).
[12] J. G. Neuman *et al.*, Nucl. Instrum. Methods Phys. Res., Sect. A **507**, 498 (2003).
[13] Y.-C. Huang, Int. J. Mod. Phys. B **21**, 287 (2007).
[14] J. G. Neumann *et al.*, in *Proceedings of the 21st Particle Accelerator Conference, Knoxville, 2005* (IEEE, Piscataway, NJ, 2005), p. 704.
[15] M. Boscolo *et al.*, Nucl. Instrum. Methods Phys. Res., Sect. A **577**, 409 (2007).
[16] L. Serafini, IEEE Trans. Plasma Sci. **24**, 421 (1996).
[17] E. Kallos *et al.*, in *Proceedings of the Advanced Accelerator Concepts 2006, Lake Geneva, WI*, AIP Conf. Proc. No. 877, edited by M. Conde and C. Eyberger (AIP, New York, 2006), p. 520.
[18] P. Schutt, T. Weiland, and V. M. Tsakanov, in *Proceedings of the Second All-Union Conference on New Methods of Charged Particle Acceleration* (Springer, New York, 1989).
[19] C. Jing *et al.*, Phys. Rev. Lett. **98**, 144801 (2007).
[20] P. Muggli *et al.*, Phys. Rev. Lett. **101**, 054801 (2008).
[21] P. Emma *et al.*, Phys. Rev. Lett. **92**, 074801 (2004).
[22] D. C. Nguyen and B. E. Carlsten, Nucl. Instrum. Methods Phys. Res., Sect. A **375**, 597 (1996).
[23] P. Piot *et al.*, AIP Conf. Proc. **1086**, 677 (2009).
[24] D. T. Palmer *et al.*, in *Proceedings of the Advanced Accelerator Concepts Workshop, Lake Tahoe, CA, 1996*, AIP Conf. Proc. No. 398, edited by S. Chattopadhyay (AIP, New York, 1997), p. 695.
[25] See, for example, W. D. Kimura *et al.*, Phys. Rev. ST Accel. Beams **4**, 101301 (2001).
[26] D. C. Carey, *The Optics of Charged Particle Beams* (Harwood Academic Publishers GmbH, Chur, Switzerland, 1992).
[27] P. Muggli *et al.*, in *Proceedings AAC08*, AIP Conf. Proc. No. 1086 (AIP, New York, 2008), p. 683.
[28] M. L. Ter-Mikaelian, *High-energy Electromagnetic Processes in Condensed Media* (Wiley-Interscience, New York, 1972).
[29] J. Wang and T. Higo, Report No. SLAC-PUB10370, 2004.
[30] FACET proposal available at http://www-group.slac.stanford.edu/ppa/Reviews/facet-review-2008/default.asp.
[31] M. J. Hogan, New J. Phys. (to be published).
[32] A. M. Cook *et al.*, Phys. Rev. Lett. **103**, 095003 (2009).
[33] J. B. Rosenzweig (private communication).
[34] V. Yakimenko *et al.*, in *Proceedings of the 23rd Particle Accelerator Conference, Vancouver, Canada, 2009* (IEEE, Piscataway, NJ, 2009).